






# Stretchable e-Skin Patch for Gesture Recognition on the Back of the Hand

Shuo Jiang , *Student Member, IEEE*, Ling Li , *Student Member, IEEE*, Haipeng Xu, *Student Member, IEEE*, Junkai Xu , *Student Member, IEEE*, Guoying Gu , *Member, IEEE*, and Peter B. Shull , *Member, IEEE*

**Abstract**—Gesture recognition is important for human–computer interaction and a variety of emerging research and commercial areas including virtual and augmented reality. Current approaches typically require sensors to be placed on the forearm, wrist, or directly across finger joints; however, they can be cumbersome or hinder human movement and sensation. In this paper, we introduce a novel approach to recognize hand gestures by estimating skin strain with multiple soft sensors optimally placed across the back of the hand. A pilot study was first conducted by covering the back of the hand with 40 small 2.5 mm reflective markers and using a high-precision camera system to measure skin strain patterns for individual finger movements. Optimal strain locations are then determined and used for sensor placement in a stretchable e-skin patch prototype. Experimental testing is performed to evaluate the stretchable e-skin patch performance in classifying individual finger gestures and American Sign Language 0–9 number gestures. Results showed classification accuracies of 95.3% and 94.4% for finger gestures and American Sign Language 0–9 gestures, respectively. These results demonstrate the feasibility of a stretchable e-skin patch on the back of the hand for hand gesture recognition and their potential to significantly enhance human–computer interaction.

**Index Terms**—Feature selection, gesture recognition, human–computer interaction, skin stretch, soft sensing.

## I. INTRODUCTION

GESTURES are a ubiquitous means of human-to-human communication [1] and have the potential to play a similarly vital role in human–computer interaction [2]. Hand gestures can act as a bridge to connect human intention to smart

Manuscript received October 24, 2018; revised March 7, 2019 and April 18, 2019; accepted April 19, 2019. Date of publication May 8, 2019; date of current version August 30, 2019. This work was supported in part by the National Natural Science Foundation of China under Grant 51875347 and Grant 51622506 and in part by the Science and Technology Commission of Shanghai Municipality under Grant 16JC1401000. (Corresponding author: Peter B. Shull.)

The authors are with the State Key Laboratory of Mechanical System and Vibration, School of Mechanical Engineering, Shanghai Jiao Tong University, Shanghai 200240, China, and L. Li, H. Xu, and G. Gu are also with the Soft Robotics and Biodesign Lab, Robotics Institute, School of Mechanical Engineering, Shanghai Jiao Tong University, Shanghai, 200240, China (e-mail: jiangshuo@sjtu.edu.cn; ling\_li@sjtu.edu.cn; xuhaipeng@sjtu.edu.cn; abcxyjk@sjtu.edu.cn; guguoying@sjtu.edu.cn; pshull@sjtu.edu.cn).

Color versions of one or more of the figures in this paper are available online at <http://ieeexplore.ieee.org>.

Digital Object Identifier 10.1109/TIE.2019.2914621

hardware and software systems for a variety of real-life applications. For example, amputees can utilize gesture intention to improve prosthesis control [3] and the hearing impaired can potentially use automated gesture recognition to enable communication with the unimpaired who do not know sign language [4]. Beyond medical applications, gesture recognition has also been used to enable in-vehicle gestural interfaces in increasingly intelligent cars [5] and for robot and quadrotor teleoperation [6], [7]. Virtual and augmented reality could also be significantly enhanced through robust and effective hand gesture recognition [8], [9].

The most widely used approach to wearable hand gesture recognition is by sensing dynamic muscle characteristics in the forearm and mapping them to hand and finger postures. Surface electromyography (sEMG) is commonly used to estimate muscle activation levels and classify hand gestures through a commercial device like the Myo armband [10] or various research prototypes [11]–[13]. sEMG can also be combined with other sensing modalities to improve classification accuracy. For example, the spatial resolution for classification can be improved by combining sEMG with near-infrared spectroscopy which monitors muscle oxygenation and perfusion [14] or with mechanomyography which detects low-frequency muscle mechanical vibrations [15]. Li *et al.* [4] combined sEMG with accelerometry to identify kinematic information in the hand and arm for classification. Ultrasound imaging has also been used to detect forearm muscle morphology for hand gesture recognition [2], [16].

The wrist is another location targeted for wearable hand gesture recognition, though it is challenging to use traditional sEMG approaches because there is significantly less muscle tissue than the forearm and is instead composed mainly of tendons and bones. Nevertheless, sEMG combined with accelerometry at the wrist has been used to effectively classify hand and surface pressing gestures [17]. Other approaches include employing barometric sensors [18], [19] or force sensing resistors [20] to estimate pressure and morphology profile changes around the wrist for various hand gestures. Truong *et al.* [21] proposed capacitance sensing to capture small skin deformations on the user's wrist and made the wristband deformable and battery free. Kawaguchi *et al.* [22] measured the electrical contact resistance change due to the deformation of the wrist. Rekimoto *et al.* [23] estimated capacitance changes via capacitance sensors at the wrist for different hand gestures. Although forearm-

and wrist-based approaches can provide a portable and intuitive interface for gesture recognition, because of the complex relationship between finger movements and forearm muscle or wrist tendon activation, the accuracy of hand gestures involving higher resolution finger angles is inherently limited.

Thus, sensors placed directly on the fingers can significantly improve hand gesture recognition accuracy. Commercial data gloves are often used, such as DataGlove family (Fifth Dimension Technologies (5DT), Irvine, CA, USA) and CyberGlove (Immersion Corporation, San Jose, CA, USA), to measure finger flexion angles. However, data gloves typically cover almost the entire hand, thus, restricting mechanoreceptive sensations along the fingers and in the fingertips and can be large and bulky making them difficult or impossible for some patients to comfortably wear [24]. Epidermal electronics [25] and artificial skin sensors [26] provide another approach for estimating finger postures. Bartlett *et al.* [27] utilized a conductive bond and proposed an efficient digital fabrication approach to create a custom skin sensor to recognize various gestures. Chossat *et al.* [28] used liquid metal to create wearable soft skin to classify hand gestures and Li *et al.* [29] used carbon grease for soft sensing to recognize American Sign Language 0–9 gestures. While placing sensors directly on the fingers can improve classification accuracy, it can also be uncomfortable and hinder finger movement, prohibiting widespread adoption. Skin deformation on the back of the hand has also been captured for hand gesture recognition [30]. Sugiura *et al.* employed photo-reflective sensors to measure the distance between the device and skin [31], though thickness and skin color can affect performance. Lin *et al.* [32] utilized 19 strain sensors on the back of the hand to directly measure skin strains; however, this paper was limited in that they only investigated limited local sensor placement and the strain sensor was used for a rigid body and was thus, not suitable for soft skin strain measurement. Currently, precise strains on the back of the hand have not been systematically investigated and there is yet to be a completely soft, stretchable sensing system on the back of the hand for hand gesture classification.

The back of the hand is well suited for sensing hand gestures. Although the back of the hand is not directly used during finger manipulation, the strain patterns of the skin on the back of the hand dynamically change as the fingers move [33]. Physiologically, the hand is often used for grasping and sensing during which the fingers and palm work in concert for grasping while fingertip mechanoreceptors sense a variety of tactile stimulations including texture, temperature, pressure, vibration, and pain [34]. In contrast, the back of the hand plays a lesser role in grasping and functional sensing. Therefore, with little interference in sensing and grasping, placing sensors on the back of the hand may be more readily acceptable in practical applications than placing sensors directly on the fingers or fingertips and solves the problem of patient's general inability to wear bulky data gloves. Also, an e-skin patch with soft sensors on the back of the hand can potentially be more easily generalized than other approaches, such as a data glove, to account for different hand sizes and to distinguish between left and right hands. A sensor patch could potentially be made irrespective of hand size and the left and right sides could be distinguished via software algorithms.

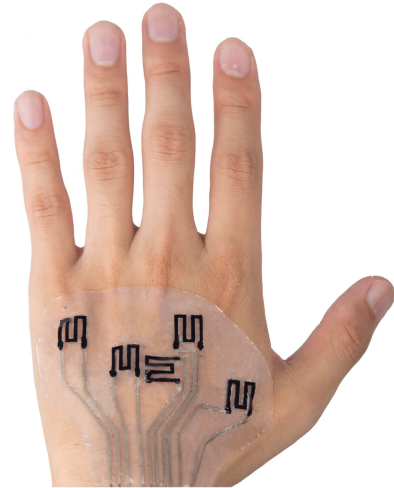


Fig. 1. Stretchable e-skin patch prototype with optimally placed soft sensors.

To achieve hand gesture recognition via sensing on the back of the hand, two key challenges must be overcome.

- 1) Skin strain complexities. In contrast with skin covering the fingers and finger joints in which skin strains are isolated to the movement of each given finger, skin strains across the back of the hand are highly coupled among several different finger movements. Thus, it is necessary to characterize back-of-the-hand skin strain patterns related to various finger movements to optimize sensor placement.
- 2) Sensor system design and manufacturing. Skin strains on the back of the hand are relatively small as compared with skin strains across the finger joints, and thus, the sensor system must be highly sensitive to the relatively small strains. In addition, the system must be designed to be small, light, and comfortable to maximize user comfort and increase the possibility of long-term compliance.

The purpose of this paper is to introduce a novel back-of-the-hand gesture recognition approach (see Fig. 1) for hand gesture classification. In contrast with previous approaches that cover the fingers and fingertips, affixing sensors to the skin on the back of hand avoids inhibiting tactile sensations. This paper addresses the inherent design and implementation challenges with an exploratory back-of-the-hand skin strain characterization experiment, a detailed prototype design, detailed algorithm development, and experimental validation. The primary contributions of this work are:

- 1) Detailed skin strain characterization across the skin on the back of the hand for various finger movements and the corresponding optimal soft sensor locations to maximize hand gesture classification accuracy.
- 2) A novel back-of-the-hand stretchable e-skin patch prototype for hand gesture recognition including soft sensor design, manufacturing, and experimental validation. To the best of our knowledge, this is the first approach combining multiple soft sensors into a stretchable e-skin patch on the back of the hand for gesture recognition.

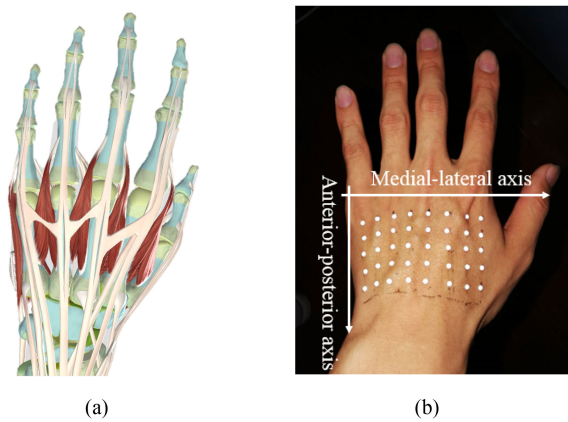


**Fig. 2.** (a) Physiological view of the back of the hand [35]. (b) Marker positions on the back of hand for the skin strain characterization experiment.

## II. BACK-OF-THE-HAND SKIN STRAIN CHARACTERIZATION

### A. Hand and Skin Physiology

The human hand is remarkably dexterous possessing approximately 25 degrees of freedom driven by muscles in the hand and forearm. The surface to the center of the hand consists of different tissues including skin, muscles, and bones. Bones act as the primary supporting structure and muscles contract to drive finger movements. Skin consists of an epidermal protective layer, an elastic dermis layer containing sensing nerves, and hypodermis layers containing fatty tissue for thermal insulation and cushioning.

Skin, muscles, and bones work together to enable dexterous hand movements. Extensor digitorum follows the metacarpal, proximal phalanx, middle phalanx, and distal phalanx [see Fig. 2(a)], and contracts during finger extension. Between each metacarpal are dorsal interosseous of the hand enabling finger flexion and abduction movements. The skin stretches with deformation during finger movements to enable lengthening and shortening of tendons and muscles. Skin stretch properties are complex because each finger movement is not driven by a single muscle, but rather by a group of synergistic, coordinated muscles activations. In addition, the skin is a single, continuous, connected organ, so individual finger movements result in coupled, nonlocalized skin stretch patterns across the hand.

### B. Experimental Protocol

To systematically analyze skin strain patterns during finger movements, an experimental protocol was designed to accurately measure an array of skin displacements on the back of the hand. A marker-based camera system approach was chosen as this has previously been shown to exhibit accurate and repeatable results [30], [36], [37]. A Simi Motion (Simi Reality Motion Systems GmbH, Unterschleißheim, Germany) motion capture system was used to quantify the complex skin strains during various finger movements. The camera sampling rate was 50 Hz, which was considered sufficiently high to capture typical finger movements at 5 Hz or less. Markers were located ac-

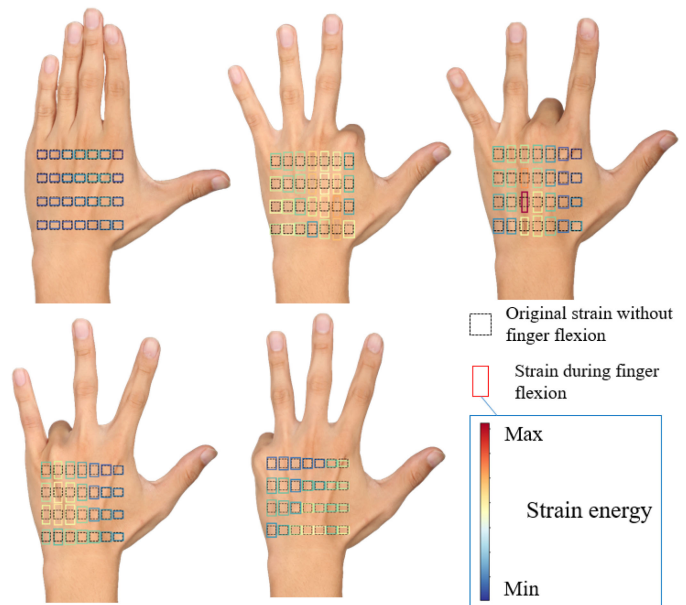


**Fig. 3.** Skin strain distribution for thumb abduction, index finger flexion, middle finger flexion, ring finger flexion, and little finger flexion. Black dashed squares represent original strains without finger flexion (upper left), colored rectangles represent strains during finger flexion. Each rectangle's width and length are proportional to medial-lateral and anterior-posterior strain at that location. Color intensity represents relative strain energy.

ording to physiological hand landmarks to enable consistency across subjects of different hand sizes. Specifically, 2.5-mm-diameter markers were attached along the second, third, fourth, fifth metacarpals and between each metacarpal in a  $5 \times 8$  rectangular grid [see Fig. 2(b)].

Ten subjects (all male, age:  $27.2 \pm 6.1$  yr, height:  $176.7 \pm 8.8$  cm, weight:  $70.5 \pm 8.3$  kg) gave informed consent and participated in this experiment which conformed with the Declaration of Helsinki. Before testing, a staff member placed markers on the back of the left hand with skin safe, adhesive gel (Safe Grip, Walker Tape, USA). We selected individual finger movements for testing (see Fig. 3) as they are the primary movements that form the foundation of hand gestures. Thus, during the experiment, subjects were asked to perform hand postures with each of the following movements: thumb abduction, index finger flexion, middle finger flexion, ring finger flexion, and little finger flexion. Each hand posture was held constantly for three seconds and each hand posture was repeated three times. Automated tracking analysis was performed posttesting via Simi Motion software to determine each marker's displacement throughout each trial.

### C. Data Analysis

Data processing was performed to transform absolute marker displacements to relative marker displacements to eliminate motion artifacts. For each gesture during each trial, the first and last one second of data were discarded to avoid transient effects, and the middle one second of steady-state data were retained for analysis. Data from all subjects were averaged together to



perform comprehensive analysis. Relative marker positions and strains were decomposed in medial-lateral ( $x$ -axis) and anterior-posterior ( $y$ -axis) directions and calculated as follows:

$$R_{x(i,j)} = d_{(i,j+1)} - d_{(i,j)} \quad (1)$$

$$R_{y(i,j)} = d_{(i+1,j)} - d_{(i,j)} \quad (2)$$

$$\epsilon_{x(i,j)} = \frac{R_{x(i,j)}^k - R_{x(i,j)}^0}{R_{x(i,j)}^0} \quad (3)$$

$$\epsilon_{y(i,j)} = \frac{R_{y(i,j)}^k - R_{y(i,j)}^0}{R_{y(i,j)}^0} \quad (4)$$

where  $R_x$ ,  $R_y$  represent the relative distance between adjacent markers in medial-lateral and anterior-posterior directions respectively,  $d_{(i,j)}$  represents the absolute displacement of the marker in  $i$ th row and  $j$ th column, and  $\epsilon_{x(i,j)}$ ,  $\epsilon_{y(i,j)}$  represent the medial-lateral and anterior-posterior local strain at each location, respectively.  $R^k$  represents relative marker distance corresponding to the  $k$ th gesture and when  $k = 0$ , it corresponds to rest-state gesture, defined as the reference length.

In addition, a strain energy metric was used and calculated as follows:

$$E_{(i,j)} = \left( \frac{|\epsilon_{x(i,j)}| + |\epsilon_{x(i+1,j)}|}{2} \right)^2 + \left( \frac{|\epsilon_{y(i,j)}| + |\epsilon_{y(i,j+1)}|}{2} \right)^2 \quad (5)$$

where  $E_{(i,j)}$  represents the strain energy of the rectangle formed by four adjacent markers and is visualized via color intensity (see Fig. 3). The color intensity is based on the normalization of all the strain energy defined in (5).

#### D. Results

Overall skin strain and strain energy characterization showed that generally, anterior-posterior strains occurred along the metacarpal of each respective finger during flexion (see Fig. 3). Medial-lateral strain was especially prominent during flexion of the little finger. Skin in the center of the back of the hand tended to have more pronounced and obvious strain patterns. Thumb abduction exhibited the smallest strain and ring finger flexion exhibited the largest strain on average. The average skin stretch (strain) in the medial-lateral direction was 0.71 mm (4.84%) and in the anterior-posterior direction was 0.90 mm (3.66%) (see Fig. 3). The largest skin stretch in the medial-lateral direction was 1.73 mm and in the anterior-posterior direction was 2.36 mm. The highest strain energy occurred during middle finger flexion near the third quartile of the third dorsal interosseous of the hand and the lowest strain energy occurred during thumb finger abduction near the fourth quartile of the fifth metacarpal.

### III. OPTIMAL SENSOR PLACEMENT DESIGN

#### A. Motivation

Building off the skin strain characterization results in the previous section, optimal sensor placement analysis was performed to maximize hand gesture classification accuracy. The distance between each adjacent pair of markers was defined as a distinct

feature corresponding to a specific skin location in either an anterior-posterior or medial-lateral orientation (67 total features for all markers across the back of the hand) and then, a subset of features was chosen to maximize classification accuracy. One method is to choose the features with maximum strain during finger movements, however, these features are not guaranteed to produce optimal classification results. Instead, features should be selected that can provide the most distinguishing information for different classes including how they are coupled together. In general, a systematic process of feature selection resulting in a subset of full feature set can reduce computational load, enhance performance, and provide better understanding of data [38] and is widely used in text categorization [39], [40], data mining [41], [42], and genomic analysis [43], [44]. In the specific case of wearable hand gesture recognition devices designed for skin on the back of the hand, feature selection can inform optimal sensor locations and reduce the total number of required sensors to enable practical implementation.

#### B. Feature Selection

The original 67 feature set was reduced to five robust features with acceptable computational load (see Fig. 4). In general, this feature reduction process involved the following steps: 1) three different feature selection methods were used to assign respective scores to each feature and reduced the total number of features to 32; 2) a Gaussian filter eliminated potential displacement errors; and 3) the final five features were chosen via a classifier calculating the performance for all the possible five feature combinations, and the highest performing combination was chosen.

Specifically, raw data comprising the full dataset were based on the experimental data collection described in Section II. Each individual feature was defined as the distance between adjacent markers. There were 32 medial-lateral features and 35 anterior-posterior features resulting in 67 total features in the full feature set [see Fig. 2(b)]. Features were scored based on the filter, wrapper, and embedded methods. The filter method is similar to preprocessing and does not require a learning algorithm. Features are generally evaluated by predefined criteria and in this case, mutual information [45], [46] was chosen based on information theory to provide more general measures of the dependency between target and feature sets [47]. A primary benefit of mutual information is that it can measure nonlinear relationships [48] unlike other methods such as the Pearson correlation coefficient. We implemented this metric via python based on entropy estimation from  $k$ -nearest neighbors (KNN) [48], [49].

Unlike filter methods, the wrapper method allows detection of possible interactions between variables [50]. Classifiers were involved in the wrapper method and the performance of the classifier was used as criteria for subset selection [51]. In this paper, the recursive feature elimination method was utilized: first, a classifier was trained using all features and then, the worst performing feature was eliminated based on model coefficients which reflected the importance of different features [52]. Then, the pruned feature subsets were used to iterate the procedure

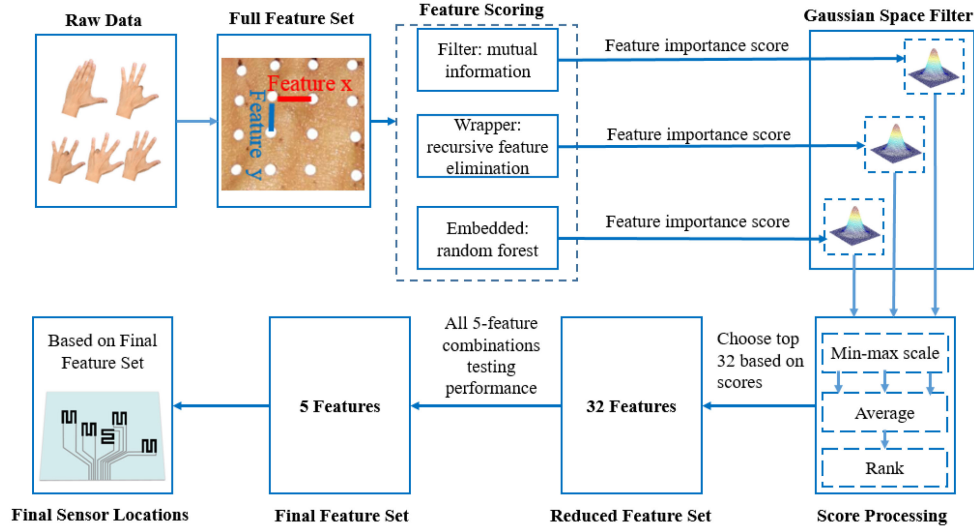


Fig. 4. Feature selection algorithm flow chart leading to optimal sensor locations.

until the feature number was reduced to a predefined minimum number (in our case, five features). After iteration, features were ranked by the order of being eliminated. Logistic regression was chosen as the predefined classifier for wrapper method in our case.

The embedded model computes feature importance scoring as the classifier is constructed. The embedded model relies on the chosen classifier and the selected optimal features via certain classifiers may differ from optimal features selected by other classifiers [53]. Random forest (RF), a commonly used classifier, is a bagging method consisting of a collection of decision tree classifiers. The intrinsic characteristic of decision trees helps to assign each feature with a score when splitting a node based on mean decrease impurity. The criterion for splitting a node is Gini impurity, which measures the probability when randomly choosing two samples that they have different labels and is defined as follows:

$$\text{Gini}(D) = \sum_{k=1}^{|y|} \sum_{k' \neq k} p_k p_{k'} = 1 - \sum_{k=1}^{|y|} p_k^2 \quad (6)$$

where  $p_k$  the probability of correctly labeling the sample with label  $k$  ( $k = 1, 2, \dots, |y|$ ) and  $p'_k$  is the probability of wrongly labeling the sample with label  $k$ . The feature score is high when the Gini index is low.

Since the markers are placed on subjects with different hand sizes, it is possible that the target markers can slightly shift to adjacent places. Thus, an algorithm which can consider the possible shifts and calculate the weighted sum of adjacent features is needed. In convolutional neural networks, convolutional layers extract features via the convolutional operation between filter and local neighbor pixels, and similarly, a Gaussian space filter was employed to compute weighted sums of adjacent features. The Gaussian space filter assigns the center point the highest weight, and the weight value decreases as the distance from the center increases. The Gaussian space filter was used for the preliminary filter, wrapper, and embedded methods. The

mathematical formulation of the Gaussian filter is defined as follows:

$$G(x, y) = \frac{1}{2\pi\sigma^2} e^{-\frac{x^2+y^2}{2\sigma^2}} \quad (7)$$

where  $\sigma$  represents the standard deviation and  $x$  and  $y$  represent the distance from the center point. In our application, we chose a  $3 \times 3$  Gaussian kernel template with a  $\sigma$  of 0.5 based on preliminary testing to ensure a reasonable and balanced weight for averaging.

The filtered score of each feature was normalized to the same range and then, the average score under different feature selection methods was used to compute the final score.

Based on preliminary testing to determine a computationally acceptable method with a reduced number of features for further processing, we chose the top 32 features. The final feature set included five features, because we assumed this was the minimum required to reconstruct each of the five independent finger movements for the simplified model of a hand, which has also been frequently adopted by other researchers for placing sensors on finger joints [29], [54]. A complete search method was adopted to find five features from 32. The criterion was the resulting accuracy of leave-one-user-out cross validation. Linear discriminant analysis (LDA) was used, because it is computationally efficient and typically performs as well as other algorithms for the given testing conditions [55], [56]. This algorithm was programmed via Python with the help of Scikit-learn module [57].

### C. Results

Based on the aforementioned analysis, the final selected features and their respective locations were:  $R_{y(1,1)}$  (first quartile of the fifth metacarpal),  $R_{y(2,3)}$  (second quartile of the fourth metacarpal),  $R_{x(3,4)}$  (middle of the third dorsal interosseous),  $R_{y(1,6)}$  (first quartile of the second dorsal interosseous),  $R_{y(3,7)}$  (third quartile of the second metacarpal) (see Fig. 1). The final sensor locations were positioned along the anterior of each metacarpal. Generally, anterior-posterior features scored more

than medial-lateral features based on the ranking for all features, and the lowest ranking features were generally located near the first quartile of the fifth metacarpal in the medial-lateral direction.

#### IV. E-SKIN PATCH SYSTEM DESIGN

##### A. e-Skin Patch Prototype

To make the e-skin patch feasible for hand gesture recognition and user friendly to become a wearable gesture interface, two criteria should be considered: 1) high sensor resolution to fulfill the requirement from Section II; and 2) sensors should be thin, skin compatible, and deformable enough to form a comfortable interface. Considering the tradeoff of sensitivity, low expense for manufacturing, and easy access for measurement, we chose to design the stretchable e-skin patch to be resistance-based type in a 3-layer structure—two outside elastomers protecting the soft electrode layer made of carbon grease (847, MG Chemical, Canada) in the middle. Each sensor unit was designed in an S-shaped pattern to enhance sensitivity as well as the capability of sensing two-dimensional stretch. Sensor resistance has a relatively good linear relationship with carbon grease strain and when the length or width stretches, the sensor's resistance will increase. The substrate was made from off-the-shelf commercial biocompatible silicone film (SILPURAN FILM 2030, thickness = 100  $\mu\text{m}$ , Wacker Chemie, Germany) which is ultrathin and permeable to air.

For manufacturing, a laser cutter was used to cut the custom designed shape on a polyethylene terephthalate (PET) film (thickness = 100  $\mu\text{m}$ ). After placing the PET film with customized shapes on silicone film, screen printing technology was utilized to fabricate carbon grease electrodes. The PET film was peeled off and the laser-cut conductive cooper-tin fabric was embedded to connect electrodes with outside electronics. A very thin Ecoflex 30 (Smooth-On, resin and harder mixed by 10:1 in weight) layer was brushed onto the silicone film as an adhesive and another silicone film was applied as the cover, which was cured for approximately 15 minutes at room temperature [see Fig. 5(a)]. After performing the loading sensor characterization test, the sensor resolution was determined to be 0.01 mm in both the anterior-posterior and medial-lateral directions and the total thickness of the e-skin patch was 550  $\mu\text{m}$ . Two experiments were performed to further investigate sensor characteristics. A cyclic loading experiment was performed in which sensors were repeatedly and continuously loaded from 0% to 100% strain. Results showed that hysteresis was 0.09 [see Fig. 5(b)]. Also, a seven-day cyclic experiment of 100 cycles per day was conducted, and results showed that the signals were stable and repeatable across days and the sensor was still sensitive on the seventh day [see Fig. 5(c)], demonstrating the potential for long-term use.

A customized circuit was designed to measure and record the resistance change. A stable power supply was applied on each electrode in series with a standard resistor. The voltage between electrode and standard resistor was measured by an analog to digital converter which transmitted the data to a computer. The

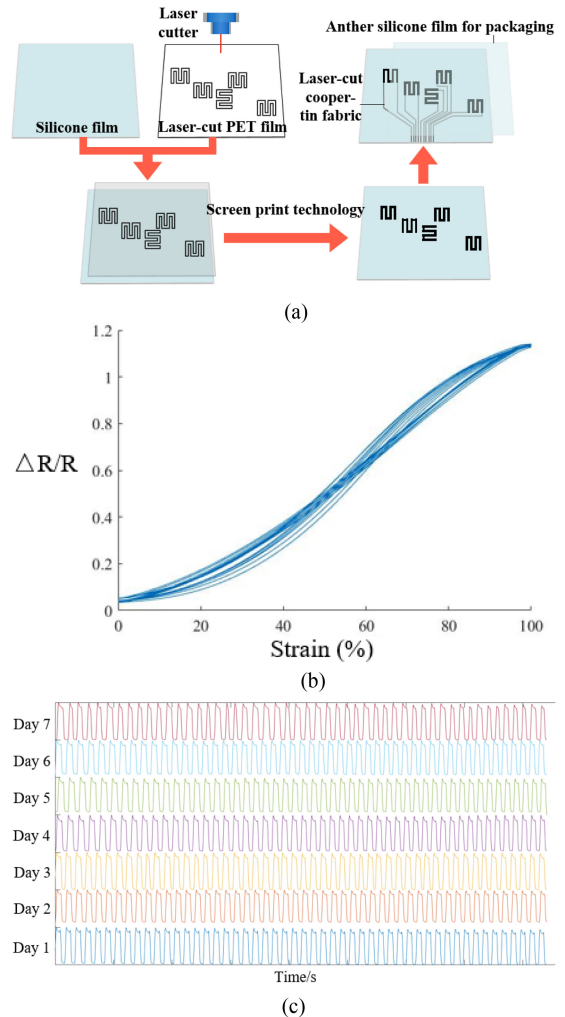


Fig. 5. (a) Stretchable e-skin patch manufacturing process. (b) Hysteresis experiment. (c) 7-day cyclic experiment.

sampling frequency was 100 Hz. Data were stored and processed on the computer.

##### B. e-Skin Patch Classification Algorithm

The electrode resistance and the sampling voltage have a clear nonlinear relationship described by  $V = \frac{(3.3 \times R_x)}{(R_0 + R_x)}$ . The sampled voltage is positively correlated to electrode resistance and is asymptotic to 3.3 V, which acts as a saturation function to suppress higher resistance values. Therefore, voltage values were chosen as features. The system had five channels and thus the feature vector was five dimensional.

For classification, LDA was chosen for its low computational load and robustness. Based on LDA, the computation time was 0.25 ms in an embedded system (STM32L475), which should theoretically be fast enough for real-time performance while sampling at 100 Hz (10 ms per cycle). LDA is based on the Bayes theory

$$Pr(G = k | X = x) = \frac{f_k(x)\pi_k}{\sum_{l=1}^K f_l(x)\pi_l} \quad (8)$$

where  $Pr(G = k|X = x)$  is the posterior probability,  $\pi_k$  is the prior probability of class  $k$ , and  $f_k(x)$  is the class conditional density. LDA tries to model the class conditional density  $f_k(x)$  with Gaussian distribution and assumes class covariance is identical. Gaussian distribution parameters such as mean and covariance are estimated in the training process.

The discriminant function is defined as

$$\delta_k(x) = x^T \Sigma^{-1} \mu_k - \frac{1}{2} \mu_k^T \Sigma^{-1} \mu_k + \log \pi_k \quad (9)$$

where  $x$  is the input vector,  $\Sigma$  is the covariance matrix,  $\mu_k$  the  $k$  class's mean, and  $\pi_k$  the prior probability of class  $k$ . Training was performed as described below to acquire the estimated prior probability and Gaussian distribution parameters via the following:

$$\hat{\pi}_k = \frac{N_k}{N} \quad (10)$$

$$\hat{\mu}_k = \frac{\sum_{g_i=k} x_i}{N_k} \quad (11)$$

$$\hat{\Sigma} = \sum_{k=1}^K \sum_{g_i=k} \frac{(x_i - \hat{\mu}_k)(x_i - \hat{\mu}_k)^T}{N - K} \quad (12)$$

where  $N_k$  is the number of class  $k$  observations. Hand gesture classification was determined based on the output function with the highest value as follows:

$$g_k(x) = \text{var} \max_l \{\delta_l(x)\}. \quad (13)$$

As a comparison, we also performed classification with other commonly used KNN and RF algorithms.

## V. EXPERIMENTAL VALIDATION

### A. Testing Protocol

An experiment was performed to evaluate the performance of the stretchable e-skin patch system for classifying various hand gestures. Eight subjects (six male, two female, age:  $27.2 \pm 6.1$  yr, height:  $176.7 \pm 8.8$  cm, weight:  $70.5 \pm 8.3$  kg) participated in the experiment after giving informed consent in accordance with the Declaration of Helsinki. A staff member attached the customized e-skin patch to the subject's left hand with skin safe, adhesive gel (Safe Grip, Walker Tape, USA). Two different groups of gestures were chosen (see Fig. 6). Group 1 was designed to validate the actual performance of the e-skin patch prototype based on sensor location optimization and the chosen gestures were the same as those in Section II—thumb abduction, index finger flexion, middle finger flexion, and ring finger flexion. Group 2 was designed to test the generalizing performance and chose potential commonly used gestures in daily life which were comprised of American Sign Language 0–9 gestures. Subjects performed the required gestures following a video guidance cueing target gesture's picture on screen for 5 s with 5 s rest in between which is the commonly used protocol in [17] and [58]. The relatively short protocol time could increase the proportion of transient state, and during transient state, classification can deteriorate because the model was trained based on steady-state signals. Each gesture appeared once per trial



Fig. 6. Validation testing hand gesture sets.

and the whole experiment consisted of ten total trials. Subjects rested after each trial, if desired, for up to 2 min.

### B. Data Analysis

Data were stored on the computer and analysis was performed offline. The first and last 0.5 second of target gesture data often included transient-state data and were thus discarded, and the middle 4 s of steady-state data were retained for analysis. The sampling frequency was 100 Hz and thus, each dataset contained 400 data samples for each gesture in each trial. A low-pass filter with a 10 Hz cutoff frequency was used to reduce high-frequency noise. Leave-one-trial-out cross validation for each subject was used to access the classification performance and two different group gestures were processed separately. The classification accuracy was defined as correctly classified sample numbers divided by total sample numbers. The Kruskal–Wallis H test, a nonparametric test that imposes no prior distribution assumption [59], [60], was utilized to determine if different classifiers had an impact on classification accuracy, and the threshold value was set to  $p = 0.05$ .

### C. Results

An example trial showed raw sensor data when performing American Sign Language digits 0–9 gestures (see Fig. 7). For finger gestures, LDA, KNN, and RF classification accuracies were  $95.3 \pm 4.0\%$ ,  $93.0\% \pm 5.4\%$ , and  $91.6 \pm 3.7\%$ , respectively. The highest accuracy for a single subject was 100%, and the lowest accuracy for a single subject was 84.4%. For American Sign language 0–9 gestures, the classification accuracy was  $94.4 \pm 2.3\%$ ,  $91.5\% \pm 3.1\%$ , and  $91.8 \pm 2.5\%$ , respectively (see Fig. 8). The highest accuracy for a single subject was 97.2% and the lowest accuracy for a single subject was 87.1%. The



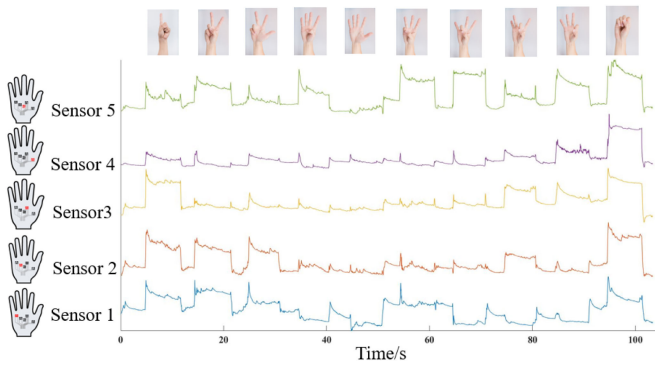


Fig. 7. Raw sensor data signals from sensors 1–5 when performing American Sign Language digits 0–9 gestures.

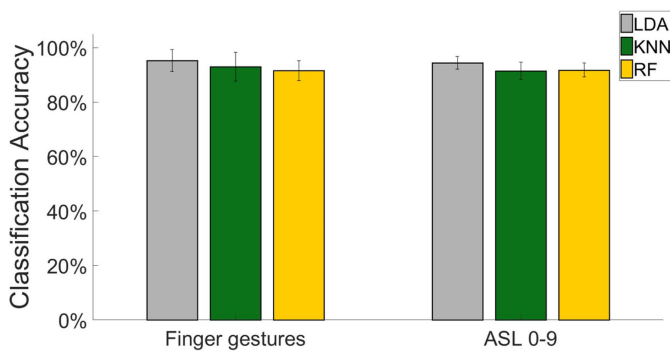


Fig. 8. Classification accuracy for different gesture sets. ASL: American Sign Language, LDA: Linear Discriminant Analysis, KNN: K Nearest Neighbors, RF: Random Forests.

Kruskal–Wallis H test results showed no significant difference among different classification methods ( $p = 0.23$ ).

## VI. DISCUSSION

This paper presents a novel wearable on-body solution for gesture recognition. Our approach to recognize hand gestures is distinct from the conventional approach of putting sensors directly on joint angles, such as for data gloves, because strains on the back of the hand are complex and coupled for different finger movements. Strain characterization was investigated and visualized with a high-precision marker-based camera system. An e-skin patch of five soft sensors on the back of the hand with geometry optimization was validated with experiments and showed promising results. Although camera and vision-based systems can achieve high precision for tracking, they present potential privacy concerns because of the visual data collected, and they are sometimes not portable when the camera needs to be mounted to a fixed location such as Leap Motion or Microsoft Kinect. Also, the background complexity and light condition can affect the results. In contrast, the wearable approach is ubiquitous without the limitation of privacy and environment complexity problem.

Carbon grease is a widely used material for sensor electrodes. Compared with liquid metal and nanoparticles, carbon grease electrodes are relatively inexpensive, decreasing the total cost of

TABLE I  
COMPARISON WITH STATE-OF-THE-ART MATERIALS

Electrode material	Gauge Factor	Price(\$/g)	Limitation
Liquid metal [61]	1-7	0.74	Injected channels; complex manufacturing
CNT [62], [63]	0.06-0.82	0.30	Complex manufacturing process
Graphene [64]	1.6-7.1	2.49	High price
Conductive ink [65]	~3.8	0.015	Injected channels; complex manufacturing process
Nanoparticles [66], [67]	~2.05	/	Expensive
Carbon grease	1.13	0.185	Relatively low Gauge Factor

the sensing system (see Table I). In addition, the manufacturing process of carbon grease-based sensors is much simpler than liquid metal electrodes, because it does not need preinstalling channels. The sensitivity of carbon grease can be relatively low but is generally high enough for most applications including gesture recognition.

Classification accuracy of the proposed system was compared to that of other wearable solutions. For example, the results were slightly higher than wrist or forearm-based methods such as sEMG and pressure [17], [18]. This may be because the sensors were located closer to finger movements with larger signal changes during finger movements. The presented classification results were slightly lower than previous ultrasonic approaches [2], [16], however, the presented experiment protocol was also significantly different, and ultrasonic methods are generally bulky and expensive. Finger joint soft sensors [29] also exhibit higher accuracies though they can impose restrictions on finger movement. Sugiura *et al.* [31] used photo-reflective sensors to measure the distance between the device and skin, and though the idea is similar, the principle is different. Our approach is to directly measure skin strains which could potentially be integrated in aesthetical e-skin or tattoo sensors for more natural, aesthetic applications. Lin *et al.* [32] utilized 19 force resistive sensors on the back of the hand for gesture classification and achieved 95.8% classification accuracy. Although the performance is similar, the following concerns and updated methods distinguish this paper from Lin's previous research: 1) their research method was only in one dimension and did not consider two-dimensional skin stretch. Instead, we used high-precision marker-based camera system to fully investigate the skin stretch properties and design our prototype sensor capable of sensing in two dimensions. As a result, the proposed system includes features in both dimensions; 2) they did not perform whole area feature selection to find a global optimum. Their methods did not consider coupling effects and sensor placement was not optimized. In contrast, we performed feature selection based on data covering the whole potential area for interaction and the sensor number was reduced to five through a systematic optimization process; and 3) their strain sensor did not conform with skin and was not user friendly. Also the strain sensor was used to measure rigid structures and thus, it is possible to damage the sensors when removing the sensors. Our soft sensors



were custom designed to be flexible, stretchable, and thin to make the e-skin patch more user friendly.

A well known problem with feature selection and the associated algorithm development is variance leading to a lack of robustness. The approach in this paper to improve robustness involved the following: 1) ten subjects were recruited to eliminate individual accidental event to ensure statistically reliable results. Also, when attaching markers on skin, different subjects had different physiological parameters such as hand size which could make the data unreliable. We studied the physiological structure of the hand and attached markers according to these landmarks so that different hand sizes could be scaled; and 2) in the feature selection algorithm, we first utilized three different approaches and calculated their mean as the preliminary feature importance score to overcome each method's certain drawbacks and limitations. Second, to reduce the possible shifting problem of attached markers and different hand parameter problem, a Gaussian filter was used to assign the center highest weight and adjacent features different lower weight according to the distance to center point. Finally, after the feature number was reduced to an acceptable computation load, we established the ten subjects' average recognition accuracy as metrics and calculated each combination of features and the corresponding classification accuracy. In this way, the coupling effect of each feature could be fully considered and the reduced feature set's global optimization was found. From the results of feature selection, the selected features frequently appeared in the top rank which demonstrated that feature selection had some robustness. In addition, four of the five optimal sensor locations were oriented to sense anterior-posterior stretch which could be attributed to the reason that hand gestures were composed of finger movements primarily driving skin stretch on the back of the hand in anterior-posterior directions. Near the middle of the third dorsal interosseous where large and irregular stretch could occur due to convergent trends of tendons was the only location of a medial-lateral stretching sensor.

Aesthetically, the back of the hand is a relatively common place for tattoos and thus, future users could potentially wear a stretchable e-skin patch with various artistic designs and patterns. Thus, the proposed prototype could potentially be leveraged to integrate both function and fashion. Thin customized aesthetic pattern layers could potentially be printed on top of the prototype enabling the motivation of widespread long term use.

The sensor is based on resistance sensing and thus, the extra power requirement for resistance sensing is relatively low compared with other embedded system components such as wireless communication [21]. Although the proposed system is promising for practical embedded systems, one potential limitation is that we have not integrated the microcontroller, power supply, and wireless communication into a stand-alone system. Future work should focus on developing battery-free and low power systems [21] or integrating e-skin with off-the-shelf smart watches and wristbands and adopting experiment protocol more similar to real-life scenarios. Future work could also consider extracting more informative features such as strain energy for gesture recognition classification.

## VII. CONCLUSION

This paper introduced a novel sensing system and the principle for gesture recognition with little interference on user's motion and sensing via stretchable e-skin patch with multiple soft sensors on the back of the hand. A high-precision marker-based camera system was used to investigate the characteristic of skin stretch with ten subjects to provide insights about skin stretch along finger movements. Based on the results, a robust feature selection method was introduced to optimize sensor locations considering the coupling effects. Finally, a customized e-skin patch with multiple soft sensors was designed, manufactured, and validated by experiment. The proposed system could facilitate future intuitive human-computer interaction.

## REFERENCES

- [1] D. McNeill, *Language and Gesture*, vol. 2, Cambridge, U.K.: Cambridge Univ. Press, 2000.
- [2] J. McIntosh, A. Marzo, M. Fraser, and C. Phillips, "Echoflex: Hand gesture recognition using ultrasound imaging," in *Proc. CHI Conf. Human Factors Comput. Syst.*, 2017, pp. 1923–1934.
- [3] W. Guo, X. Sheng, H. Liu, and X. Zhu, "Toward an enhanced human-machine interface for upper-limb prosthesis control with combined EMG and NIRS signals," *IEEE Trans. Human-Mach. Syst.*, vol. 47, no. 4, pp. 564–575, Aug. 2017.
- [4] Y. Li, X. Chen, X. Zhang, K. Wang, and Z. J. Wang, "A sign-component-based framework for Chinese sign language recognition using accelerometer and sEMG data," *IEEE Trans. Biomed. Eng.*, vol. 59, no. 10, pp. 2695–2704, Oct. 2012.
- [5] E. Ohn-Bar and M. M. Trivedi, "Hand gesture recognition in real time for automotive interfaces: A multimodal vision-based approach and evaluations," *IEEE Trans. Intell. Transp. Syst.*, vol. 15, no. 6, pp. 2368–2377, Dec. 2014.
- [6] K. Qian, J. Niu, and H. Yang, "Developing a gesture based remote human-robot interaction system using Kinect," *Int. J. Smart Home*, vol. 7, no. 4, pp. 203–208, 2013.
- [7] A. Mashood, H. Noura, I. Jawhar, and N. Mohamed, "A gesture based Kinect for quadrotor control," in *Proc. Int. Conf. Inf. Commun. Technol. Res.*, 2015, pp. 298–301.
- [8] M. Billingham, T. Piumsomboon, and H. Bai, "Hands in space: Gesture interaction with augmented-reality interfaces," *IEEE Comput. Graph. Appl.*, vol. 34, no. 1, pp. 77–80, Jan./Feb. 2014.
- [9] K. M. Sagayam and D. J. Hemant, "Hand posture and gesture recognition techniques for virtual reality applications: A survey," *Virtual Reality*, vol. 21, no. 2, pp. 91–107, 2017.
- [10] Thalmic Labs, "Myo—Gesture control armband by Thalmic Labs," 2013. [Online]. Available: <https://support.getmyo.com/hc/en-us>
- [11] Z. Ju and H. Liu, "Human hand motion analysis with multisensory information," *IEEE/ASME Trans. Mechatronics*, vol. 19, no. 2, pp. 456–466, Apr. 2014.
- [12] S. Benatti *et al.*, "A versatile embedded platform for EMG acquisition and gesture recognition," *IEEE Trans. Biomed. Circuits Syst.*, vol. 9, no. 5, pp. 620–630, Oct. 2015.
- [13] G. Yang *et al.*, "An IoT-enabled stroke rehabilitation system based on smart wearable armband and machine learning," *IEEE J. Transl. Eng. Health Med.*, vol. 6, pp. 1–10, 2018.
- [14] W. Guo, X. Sheng, H. Liu, and X. Zhu, "Development of a multi-channel compact-size wireless hybrid sEMG/NIRS sensor system for prosthetic manipulation," *IEEE Sensors J.*, vol. 16, no. 2, pp. 447–456, Jan. 2016.
- [15] W. Guo, X. Sheng, H. Liu, and X. Zhu, "Mechanomyography assisted myoelectric sensing for upper-extremity prostheses: A hybrid approach," *IEEE Sensors J.*, vol. 17, no. 10, pp. 3100–3108, May 2017.
- [16] Y. Huang, X. Yang, Y. Li, D. Zhou, H. Liu, and K. He, "Ultrasound-based sensing models for finger motion classification," *IEEE J. Biomed. Health Inform.*, vol. 22, no. 5, pp. 1395–1405, Sep. 2018.
- [17] S. Jiang *et al.*, "Feasibility of wrist-worn, real-time hand and surface gesture recognition via sEMG and IMU sensing," *IEEE Trans. Ind. Inform.*, vol. 14, no. 8, pp. 3376–3385, Aug. 2018.

- [18] Y. Zhu, S. Jiang, and P. B. Shull, "Wrist-worn hand gesture recognition based on barometric pressure sensing," in *Proc. IEEE 15th Int. Conf. Wearable Implantable Body Sensor Netw.*, Las Vegas, NV, USA, 2018, pp. 181–184.
- [19] P. B. Shull, S. Jiang, Y. Zhu, and X. Zhu, "Hand gesture recognition and finger angle estimation via wrist-worn modified barometric pressure sensing," *IEEE Trans. Neural Syst. Rehabil. Eng.*, vol. 27, no. 4, pp. 724–732, Apr. 2019.
- [20] A. Dementyev and J. A. Paradiso, "Wristflex: Low-power gesture input with wrist-worn pressure sensors," in *Proc. 27th Annu. ACM Symp. User Interface Softw. Technol.*, 2014, pp. 161–166.
- [21] H. Truong *et al.*, "Capband: Battery-free successive capacitance sensing wristband for hand gesture recognition," in *Proc. 16th ACM Conf. Embedded Netw. Sensor Syst.*, 2018, pp. 54–67.
- [22] J. Kawaguchi, S. Yoshimoto, Y. Kuroda, and O. Oshiro, "Estimation of finger joint angles based on electromechanical sensing of wrist shape," *IEEE Trans. Neural Syst. Rehabil. Eng.*, vol. 25, no. 9, pp. 1409–1418, Sep. 2017.
- [23] J. Rekimoto, "GestureWrist and GesturePad: unobtrusive wearable interaction devices," in *Proc. 5th Int. Symp. Wearable Comput.*, 2001, pp. 21–27.
- [24] L. K. Simone, N. Sundarajan, X. Luo, Y. Jia, and D. G. Kamper, "A low cost instrumented glove for extended monitoring and functional hand assessment," *J. Neurosci. Methods*, vol. 160, no. 2, pp. 335–348, 2007.
- [25] D.-H. Kim *et al.*, "Epidermal electronics," *Science*, vol. 333, no. 6044, pp. 838–843, 2011.
- [26] Y.-L. Park, B.-R. Chen, and R. J. Wood, "Design and fabrication of soft artificial skin using embedded microchannels and liquid conductors," *IEEE Sensors J.*, vol. 12, no. 8, pp. 2711–2718, Aug. 2012.
- [27] M. D. Bartlett, E. J. Markvicka, and C. Majidi, "Rapid fabrication of soft, multilayered electronics for wearable biomonitoring," *Adv. Functional Mater.*, vol. 26, no. 46, pp. 8496–8504, 2016.
- [28] J.-B. Chossat, Y. Tao, V. Duchaine, and Y.-L. Park, "Wearable soft artificial skin for hand motion detection with embedded microfluidic strain sensing," in *Proc. IEEE Int. Conf. Robot. Autom.*, Seattle, WA, USA, 2015, pp. 2568–2573.
- [29] L. Li, S. Jiang, P. B. Shull, and G. Gu, "SkinGest: Artificial skin for gesture recognition via filmy stretchable strain sensors," *Adv. Robot.*, vol. 32, pp. 1112–1121, 2018.
- [30] Y. Wang, K. Sun, L. Sun, C. Yu, and Y. Shi, "SkinMotion: What does skin movement tell us?" in *Proc. ACM Int. Joint Conf. Pervasive Ubiquitous Comput., Adjunct*, 2016, pp. 914–917.
- [31] Y. Sugiura, F. Nakamura, W. Kawai, T. Kikuchi, and M. Sugimoto, "Behind the palm: Hand gesture recognition through measuring skin deformation on back of hand by using optical sensors," in *Proc. 56th Annu. Conf. Soc. Instrum. Control Eng. Jpn.*, 2017, pp. 1082–1087.
- [32] J.-W. Lin *et al.*, "Backhand: Sensing hand gestures via back of the hand," in *Proc. 28th Annu. ACM Symp. User Interface Softw. Technol.*, 2015, pp. 557–564.
- [33] J. Barron, "The structure and function of the skin of the hand," *Hand*, vol. 2, no. 2, pp. 93–96, 1970.
- [34] J. Z. Wu, R. G. Dong, S. Rakheja, A. Schopper, and W. Smutz, "A structural fingertip model for simulating of the biomechanics of tactile sensation," *Med. Eng. Phys.*, vol. 26, no. 2, pp. 165–175, 2004.
- [35] 3D4Medical, "Complete anatomy," 2018. [Online]. Available: <https://3d4medical.com/apps/complete-anatomy>
- [36] K. Bark, J. Wheeler, P. Shull, J. Savall, and M. Cutkosky, "Rotational skin stretch feedback: A wearable haptic display for motion," *IEEE Trans. Haptics*, vol. 3, no. 3, pp. 166–176, Jul./Sep. 2010.
- [37] K. K. A. Bethke, "The second skin approach: Skin strain field analysis and mechanical counter pressure prototyping for advanced spacesuit design," Ph.D. dissertation, Massachusetts Institute of Technology, 2005.
- [38] G. Chandrashekar and F. Sahin, "A survey on feature selection methods," *Comput. Elect. Eng.*, vol. 40, no. 1, pp. 16–28, 2014.
- [39] R. H. Pinheiro, G. D. Cavalcanti, and T. I. Ren, "Data-driven global-ranking local feature selection methods for text categorization," *Expert Syst. Appl.*, vol. 42, no. 4, pp. 1941–1949, 2015.
- [40] B. Tang, S. Kay, and H. He, "Toward optimal feature selection in naive Bayes for text categorization," 2016, *arXiv:1602.02850*.
- [41] F. N. Koutanaei, H. Sajedi, and M. Khanbabaee, "A hybrid data mining model of feature selection algorithms and ensemble learning classifiers for credit scoring," *J. Retailing Consum. Serv.*, vol. 27, pp. 11–23, 2015.
- [42] S. Fong, R. Wong, and A. Vasilakos, "Accelerated PSO swarm search feature selection for data stream mining big data," *IEEE Trans. Serv. Comput.*, vol. 9, no. 1, pp. 33–45, Jan./Feb. 2016.
- [43] E. A. Perez *et al.*, "Genomic analysis reveals that immune function genes are strongly linked to clinical outcome in the North Central Cancer Treatment Group n9831 Adjuvant Trastuzumab Trial," *J. Clin. Oncol.*, vol. 33, no. 7, pp. 701–708, 2015.
- [44] M. L. Bermingham *et al.*, "Application of high-dimensional feature selection: Evaluation for genomic prediction in man," *Sci. Rep.*, vol. 5, 2015, Art. no. 10312.
- [45] J. R. Vergara and P. A. Estévez, "A review of feature selection methods based on mutual information," *Neural Comput. Appl.*, vol. 24, no. 1, pp. 175–186, 2014.
- [46] B. Guo and M. S. Nixon, "Gait feature subset selection by mutual information," *IEEE Trans. Syst., Man, Cybern., A, Syst. Humans*, vol. 39, no. 1, pp. 36–46, Jan. 2009.
- [47] H. Peng, F. Long, and C. Ding, "Feature selection based on mutual information: Criteria of max-dependency, max-relevance, and min-redundancy," *IEEE Trans. Pattern Anal. Mach. Intell.*, vol. 27, no. 8, pp. 1226–1238, Aug. 2005.
- [48] T. M. Cover and J. A. Thomas, *Elements of Information Theory*. Hoboken, NJ, USA: Wiley, 2012.
- [49] B. C. Ross, "Mutual information between discrete and continuous data sets," *PLoS One*, vol. 9, no. 2, 2014, Art. no. e87357.
- [50] T. M. Phuong, Z. Lin, and R. B. Altman, "Choosing SNPs using feature selection," *J. Bioinform. Comput. Biol.*, vol. 4, no. 2, pp. 241–257, 2006.
- [51] R. Kohavi and G. H. John, "Wrappers for feature subset selection," *Artif. Intell.*, vol. 97, no. 1/2, pp. 273–324, 1997.
- [52] I. Guyon, J. Weston, S. Barnhill, and V. Vapnik, "Gene selection for cancer classification using support vector machines," *Mach. Learn.*, vol. 46, no. 1/3, pp. 389–422, 2002.
- [53] Z. M. Hira and D. F. Gillies, "A review of feature selection and feature extraction methods applied on microarray data," *Adv. Bioinform.*, vol. 2015, Art. no. 198363.
- [54] J. Shintake, E. Piskarev, S. H. Jeong, and D. Floreano, "Ultrastretchable strain sensors using carbon black-filled elastomer composites and comparison of capacitive versus resistive sensors," *Adv. Mater. Technol.*, vol. 3, no. 3, 2018, Art. no. 1700284.
- [55] K. Englehart and B. Hudgins, "A robust, real-time control scheme for multifunction myoelectric control," *IEEE Trans. Biomed. Eng.*, vol. 50, no. 7, pp. 848–854, Jul. 2003.
- [56] N. Wang, Y. Chen, and X. Zhang, "The recognition of multi-finger prehensile postures using LDA," *Biomed. Signal Process. Control*, vol. 8, no. 6, pp. 706–712, 2013.
- [57] F. Pedregosa *et al.*, "Scikit-learn: Machine learning in Python," *J. Mach. Learn. Res.*, vol. 12, pp. 2825–2830, 2011.
- [58] J. McIntosh, C. McNeill, M. Fraser, F. Kerber, M. Löchtfeld, and A. Krüger, "Empress: Practical hand gesture classification with wrist-mounted EMG and pressure sensing," in *Proc. CHI Conf. Human Factors Comput. Syst.*, 2016, pp. 2332–2342.
- [59] W. H. Kruskal and W. A. Wallis, "Use of ranks in one-criterion variance analysis," *J. Amer. Statist. Assoc.*, vol. 47, no. 260, pp. 583–621, 1952.
- [60] B. J. Feir-Walsh and L. E. Toothaker, "An empirical comparison of the ANOVA F-test, normal scores test and Kruskal–Wallis test under violation of assumptions," *Educ. Psychol. Meas.*, vol. 34, no. 4, pp. 789–799, 1974.
- [61] Y.-H. Wu *et al.*, "Interface design for enhancing the wettability of liquid metal to polyacrylate for intrinsically soft electronics," *J. Mater. Chem. C*, vol. 6, no. 25, pp. 6755–6763, 2018.
- [62] T. Yamada *et al.*, "A stretchable carbon nanotube strain sensor for human-motion detection," *Nature Nanotechnol.*, vol. 6, no. 5, pp. 296–301, 2011.
- [63] M. Amjadi, Y. J. Yoon, and I. Park, "Ultra-stretchable and skin-mountable strain sensors using carbon nanotubes-Ecoflex nanocomposites," *Nanotechnol.*, vol. 26, no. 37, 2015, Art. no. 375501.
- [64] Y. R. Jeong, H. Park, S. W. Jin, S. Y. Hong, S.-S. Lee, and J. S. Ha, "Highly stretchable and sensitive strain sensors using fragmented graphene foam," *Adv. Functional Mater.*, vol. 25, no. 27, pp. 4228–4236, 2015.
- [65] J. T. Muth *et al.*, "Embedded 3D printing of strain sensors within highly stretchable elastomers," *Adv. Mater.*, vol. 26, no. 36, pp. 6307–6312, 2014.
- [66] J. Lee, S. Kim, J. Lee, D. Yang, B. C. Park, S. Ryu, and I. Park, "A stretchable strain sensor based on a metal nanoparticle thin film for human motion detection," *Nanoscale*, vol. 6, no. 20, pp. 11 932–11 939, 2014.
- [67] I. Park *et al.*, "Nanoscale patterning and electronics on flexible substrate by direct nanoimprinting of metallic nanoparticles," *Adv. Mater.*, vol. 20, no. 3, pp. 489–496, 2008.



**Shuo Jiang** (S'16) received the B.S. degree in mechatronic engineering from Zhejiang University, Hangzhou, China, in 2015. He is currently working toward the Ph.D. degree in mechanical engineering from the School of Mechanical Engineering, Shanghai Jiao Tong University, Shanghai, China.

His research interests include wearable electronics and multisensor fusion for intuitive human–computer interaction.



**Ling Li** (S'17) received the B.S. and M.S. (Hons.) degrees in mechanical and power engineering from Shanghai Jiao Tong University, Shanghai, China, in 2016 and 2019, respectively.

His research interests include movement sensing with soft strain and haptic sensors.



**Haipeng Xu** (S'18) received the B.S. (Hons.) degree in mechanical engineering from Northeastern University, Shenyang, China, in 2015. He is currently working toward the M.S. degree in mechanical engineering with Shanghai Jiao Tong University, Shanghai, China.

His research interests include three-dimensional (3-D)-printing soft sensors and robots.



**Junkai Xu** (S'18) received the B.S. degree in material forming and control engineering from Nanchang University, Nanchang, China, in 2011, and the M.S. degree in mechatronic engineering from Shangdong University, Jinan, China, in 2014. He is currently working toward the Ph.D. degree in mechanical engineering with the State Key Laboratory of Mechanical System and Vibration, School of Mechanical Engineering, Shanghai Jiao Tong University, Shanghai, China.

His research interests include wearable electronics, human motion sensing, and training.



**Guoying Gu** (S'10–M'13) received the B.E. (Hons.) degree in electronic science and technology and the Ph.D. (Hons.) degree in mechatronic engineering from Shanghai Jiao Tong University, Shanghai, China, in 2006 and 2012, respectively.

Since 2012, he has been with Shanghai Jiao Tong University, where he is currently a Professor with the School of Mechanical Engineering. He was a Humboldt Postdoctoral Fellow with the University of Oldenburg, Oldenburg, Germany.

He was a Visiting Scholar with the Massachusetts Institute of Technology, National University of Singapore, and Concordia University, Quebec, USA. His research interests include soft robotics, smart materials actuated systems, bioinspired robot design, and motion control. He is the Author or Co-Author of more than 80 publications, which have appeared in *Science Robotics*, IEEE/AMERICAN SOCIETY OF MECHANICAL ENGINEERS (ASME) TRANSACTIONS, *Advanced Functional Materials*, *Soft Robotics*, as book chapters, and in conference proceedings.

Dr. Gu is the recipient of multiple awards, including the Young Changjiang Scholar of the Ministry of Education, National Science Fund for Excellent Young Scholars, The First Prize of Natural Science of the Ministry of Education, Best Paper Award at the International Conference on Intelligent Robotics and Applications (ICIRA 2016), in 2016, and the IEEE International Conference on Information and Automation (IEEE-ICIA 2011) in 2011. He is a Member of ASME. He is currently an Editorial Board Member of the *International Journal of Advanced Robotic Systems* and Topic Editor for *Frontiers in Robotics and AI*. He has also been the General Chair of the International Symposium on Theory and Technology of Soft Robotics, in 2017 and several international conferences/symposiums as the chair, associate editor, or program committee member.



**Peter B. Shull** (M'10) received the B.S. degree in mechanical engineering and computer engineering from LeTourneau University, Longview, TX, USA, in 2005, and the M.S. and Ph.D. degrees in mechanical engineering from Stanford University, Stanford, CA, USA, in 2008 and 2012, respectively.

From 2012 to 2013, he was a Postdoctoral Fellow with the Bioengineering Department of Stanford University. He is currently an Associate Professor of mechanical engineering with

Shanghai Jiao Tong University, Shanghai, China. His research interests include wearable systems, real-time movement sensing and feedback, hand gesture recognition, and biomechanics.